Investigation of charge transport properties of [1]Benzothieno[3,2-b][1]-benzothiophene single-crystals in field-effect transistor configuration

Xiao Liu, Xiaolu Su, Clément Livache, Lise-Marie Chamoreau, Sébastien Sanaur, Lydia Sosa-Vargas, Jean-Charles Ribierre, David Kreher, Emmanuel Lhuillier, Emmanuelle Lacaze, et al.

Investigation of charge transport properties of [1]Benzothieno[3,2-b][1]-benzothiophene single-crystals in field-effect transistor configuration

Xiao Liu [a,b], Xiaolu Su [a], Clément Livache [b], Lise-Marie Chamoreau [a], Sebastien Sanaur [c], Lydia Sosa-Vargas [a], Jean-Charles Ribierre [d], David Kreher [a], Emmanuel Lhuillier [b], Emmanuelle Lacaze [b], Fabrice Mathevet [a,*]

[a] *Sorbonne Universités, Faculté des Sciences, CNRS, Institut Parisien de Chimie Moléculaire (IPCM), UMR 8232, 4 Place Jussieu, 75005 Paris, France*
[b] *Sorbonne Universités, Faculté des Sciences, CNRS, Institut des NanoSciences de Paris (INSP), UMR 7588, 4 Place Jussieu, 75005 Paris, France*
[c] *IMT Mines Saint-Etienne, Provence Microelectronics Center, Department of Flexible Electronics, 13541 Gardanne, France*
[d] *State Key Laboratory of Modern Optical Instrumentation, College of Optical Science and Engineering, Zhejiang University, Hangzhou 310027, China*

** Corresponding author: fabrice.mathevet@upmc.fr*

Keywords: Semiconducting Materials, Thienoacene derivative, Single crystals, Organic field effect transistors

Abstract Single-crystals of unsubstituted [1]Benzothieno[3,2-b][1]-benzothiophene (BTBT) were prepared by physical vapor transport deposition (VTP). The packing structure and morphology of the crystals were studied by X-ray diffraction (XRD), polarized optical microscopy (POM), scanning electron microscopy (SEM) and atomic force microscopy (AFM). The charge transport properties of BTBT single-crystals were also investigated via bottom contact/bottom gate (BC/BG) organic field-effect transistors (OFETs) on both SiO_2 and *n*-octadecyltrichlorosilane (OTS) treated surfaces. A maximum hole mobility value of 0.032 $cm^2V^{-1}s^{-1}$ was measured on the OTS substrate. In addition, single-crystal OFETs with ion gel top gate (TG) configuration were also investigated for low voltage operation. This work represents the first investigation of charge carrier mobility of a simple BTBT in transistor configuration and highlights the essential role of the BTBT substitution in charge transport properties.

1. Introduction

Organic semiconductors have attracted much attention as semiconducting materials for the development of the new generation of electronic and optoelectronic devices [1] such as organic light emitting diodes [2], organic photovoltaics [3] or organic field effect transistors (OFETs) [4–6]. Among the large amount of high-performance semiconducting materials developed so far, thienoacenes such as [1]Benzothieno[3,2-b][1]-benzothiophene (BTBT) derivatives have emerged as promising materials for the fabrication of efficient OFETs [7]. These derivatives are composed of fused thiophenes and benzene rings, leading to a rigid and planar π-conjugated system. Such chemical structure induces a large intermolecular orbital overlap in solid state explaining their high charge-carrier mobility.

Takimiya *et al.* firstly reported field effect transistor (FET) mobilities based on symmetrically substituted BTBT derivatives, end-capped either by two phenyl rings (DPh-

BTBT) or two alkyl chains (C_n-BTBT-C_n) [8, 9]. In these pioneer works, Dph-BTBT and C_n-BTBT-C_n thin films obtained by vacuum deposition and spin coating respectively, showed promising hole mobility values about 1-2 $cm^2V^{-1}s^{-1}$. Later on, the charge transport properties of alkyl-substituted BTBT derivatives were intensively studied in different FET configurations and highlighted the beneficial effect of the alkyl functionalization of the BTBT core on the charge transport properties. Hole mobilities as high as 31 $cm^2V^{-1}s^{-1}$ were demonstrated based on single-crystalline thin films of C_8-BTBT-C_8 derivative [10]. In the same way, asymmetrically alkyl-substituted BTBTs (C_n-BTBTs) and its derivatives were also widely investigated in FET configuration. For example, high mobilities about 14.7 $cm^2V^{-1}s^{-1}$ based on liquid crystalline Ph-BTBT-C_{10} spin-coated film [11], or about 17.2 $cm^2V^{-1}s^{-1}$ based on evaporated films of mono-substituted C_{13}-BTBT were obtained [12].

Recently, the local intrinsic charge carrier transport of a set of C_n-BTBT-C_n isomers was also studied by field-induced time-resolved microwave conductivity (FI-TRMC) technique. In this work, an impressive value of 145.6 $cm^2V^{-1}s^{-1}$ was first predicted via band-transport theoretical calculations with the C_{12}-BTBT-C_{12} derivatives, and an unprecedented mobility of 170 $cm^2V^{-1}s^{-1}$ was experimentally achieved [13].

To better understand the crucial role of alkyl substitution on BTBT derivative charge transport properties, Minemawari *et al*. investigated most recently the systematic chain-length dependence of the molecular packing for a series of symmetrically and asymmetrically alkyl-substituted BTBTs [14]. Based on crystal structure analyses and calculations of intermolecular interaction energies for C_n-BTBT-C_n derivatives, the authors demonstrated that substitutions with long alkyl chains stabilize the layered-herringbone packing of BTBT cores, and are consistent with the high charge carrier mobilities reported so far. In addition to these results, Yavuz *et al.* proposed to theoretically explore these structures and to rationalize the impact of alkyl substitution on bulk structure and charge-transport properties [15]. Based on solid-state morphology predicted by molecular dynamics simulations from reported X-ray crystal structures, the authors modeled charge transport by both band and hopping type transport models for each C_n-BTBT-C_n derivative. They compared these calculated mobilities with the corresponding experimental ones reported in the literature [7][9][15]. In this latter work, the charge transport properties of the unsubstituted BTBT derivative (i.e. for n=0) was also calculated, and mobility values ranging from 10^{-3} to 10^{-1} $cm^2V^{-1}s^{-1}$ were determined depending on type transport models. However, to the best of our knowledge, no comparison between experimental and theoretical field effect mobility has been reported so far for a simple BTBT unit. The absence of FET mobility values on the BTBT model is explained by the fact that homogeneous thin films of such a small heteroaromatic system cannot be obtained by vacuum vapor deposition as reported by Takimiya [16].

In this context, we report here the first investigation of charge transport properties of a simple BTBT aromatic core in transistor configuration. To overcome the inability to obtain homogeneous thin films by vacuum deposition techniques, BTBT single crystals were successfully fabricated by physical vapor transport deposition [17]. The molecular packing and morphologies of BTBT single-crystals were analyzed by X-ray diffraction (XRD), and polarized optical microscopy (POM), scanning electron microscopy (SEM), and atomic force microscopy (AFM). The BTBT single-crystals were then transferred as active layers of

bottom contact/bottom gate (BC/BG) transistors, and the charge transport properties were investigated with either SiO_2 or *n*-octadecyltrichlorosilane (OTS) treated surfaces. Hole mobility values as high as $3.2x10^{-2}$ $cm^2V^{-1}s^{-1}$ were obtained in good agreement with the modeled charge-transport properties [15]. In addition, bottom contact/top gate (BC/TG) single-crystal OFETs (SCOFETs) with ion gels gate configuration were also investigated for low voltage operation. To date, this study reports the first investigation of the FET mobility of the unsubstituted BTBT aromatic core and confirms the important role of the BTBT substitution to achieve high charge carrier mobility.

2. Experimental section

2.1 Materials

All materials and solvents were purchased from Sigma Aldrich and were used without further purification. BTBT derivative was synthesized in a one-step reaction from the commercially available 2-chlorobenzaldehyde according to the procedure described in the literature [18]. Yield: 35%. Mp=117-119 °C. ^{1}H NMR ($CDCl_3$, 200 MHz): δH = 7.95-7.87 ppm (4H, m, H_{arom}), 7.51-7.37 ppm (4H, m, H_{arom}).

2.2 Single crystal preparation

The fabrication of BTBT single crystals was adapted from the physical vapor transport deposition method reported by Laudise [17]. Several milligrams of BTBT compound were placed on a clean glass substrate and topped with another glass substrate in the hot-stage of a polarized optical microscope (Linkan THMS 350). The system was heated to 165 °C at the rate of 30 °C /min under a nitrogen flow, and kept at this temperature for 8 mins. This led to the rapid sublimation of the compound to form large, thin, single crystal platelets growing perpendicularly to the top (cold) glass substrate. The system was then cooled to room temperature at the rate of 30 °C /min. With the help of the POM, selected BTBT single crystals were carefully transferred with a microscale gold wire onto the interdigitated electrodes of transistors.

2.3 Thermal behavior

Differential scanning calorimetry (DSC) was performed using TA instruments Q2000 under N_2 flow in aluminum hermetic pans. The DSC traces of BTBT compound on heating and cooling were recorded with a rate of 2.5 °C/min, 5 °C/min, 10 °C/min and 20 °C/min respectively.

2.4 Polarized optical microscopy and scanning electron microscopy

POM was carried out using a Leica microscope equipped with a Linkan THMS 350 hot plate connected to a Linkam 93 temperature controller. The bottom contact/bottom gate (BC/BG) SCOFET devices were observed with Hitachi SEM (SU8000).

2.5 X-ray diffraction

A single crystal of BTBT was selected, mounted onto a cryoloop, and transferred under a cold nitrogen gas stream. Intensity data were collected with a BRUKER Kappa-APEXII

diffractometer with micro-focused Cu-Kα radiation at 200 °K. APEX 3 suite and SAINT program (BRUKER) were used to carry out data collection, unit-cell parameters refinement, integration and data reduction. SADABS (BRUKER) was used for scaling and multi-scan absorption corrections. Despite large diffraction peaks in some direction due to the shape of crystal, in the Olex2 suite [19], the structure were solved with SHELXT-14 [20] program and refined by full-matrix least-squares methods using SHELXL-14 [21]. CCDC 1956856 contain the supplementary crystallographic data for this paper. The data can be obtained free of charge from The Cambridge Crystallographic Data Centre via www.ccdc.cam.ac.uk/structures.

2.6 Atomic force microscopy

AFM experiments were carried out to examine the surface morphologies of BTBT single crystals. These measurements were performed in the tapping mode, with Bruker 3100 stand alone. Tips were in silicon, associated with a resonance around 300 kHz.

2.7 Fabrication and characterization of OFET devices

BC/BG transistors were fabricated on heavily-doped Silicon (Si) wafer (i.e low bulk resistivity 0.01 Ω.cm) thermally oxidized by a 280nm-thick Silicon Oxide (SiO_2) layer, purchased from MicroChemicals GmbH. SiO_2 was used here as gate dielectric (i.e Gate capacitance C_i = 12 nF/cm^2) and the Si wafer as Gate electrode in back contact. The interdigitated Source and Drain electrodes were patterned by photolithography process-flow through a MJB-4 (Karl Suss) mask-aligner in vacuum contact, and completed by lift-off technique in acetone overnight. Previously, a sequential thermal evaporation of a 5 nm-thick adhesion layer of Chromium and a 100 nm-thick Gold layer in a vacuum chamber at 10^{-7} Torr wase achieved. The channel length (L) was 2.5µm, 5µm, 12.5µm, 25µm or 50µm, while the channel width (W) depended on the size of each single crystal. The substrates were sonicated in ethanol, acetone and chloroform successively. Then they were cleaned for 30 min in a UV-Ozone cleaner. For the preparation of the OTS-treated surface, the substrates were further treated as the procedures described elsewhere [22]. Note that no top contact configuration was investigated on BTBT single crystals because of the easy sublimation of crystals at low pressure, as for example in the vacuum chamber of a metal evaporator.

Current-voltage measurements of the BC/BG OFETs were collected in the glove box (N_2 environment) using two Keithley 2400 source units and a MS Tech probe station (MST 8000). For top gate we use ion gel electrolyte [23]. The latter is obtained by mixing 50 mg of $LiClO_4$ with 230mg of polyethylene glycol (PEG, 6kg/mol) on a hot plate in an N_2-filled glovebox at 175 °C for 90 min until the solution appears clear [24]. Then mixture was cooled down and stored in the glove box to be used later. To prepare the top gate dielectric layer, the electrolyte is softened on a hot plate at 80 °C and brushed onto the channel area of the device. The device is finally cooled in the glove box first and then dried under vacuum. The PEG drops formed well-defined physical gels through non-covalent association where ether crown surround the ion and their reorganization will ensure the ion migration. A copper grid was then deposited on the top of the electrolyte gel drop to be used as the gate electrode during the current-voltage measurement in the glove box. The schematics representations of the BC/BG and BC/TG OFET structures are shown in Fig.S1 (A) and (B), and a picture of a

BC/TG transistor with ion gel drop on the top is given in Fig. S1(C).

Transfer characteristics of BG devices were acquired at V_{DS} = -20 V while V_{GS} was stepped from 5 V to -40 V in 0.5 V increments. Output characteristics of BG devices were taken at V_{GS} = 0 V to -40V in 10 V increments and V_{DS} was stepped from 0 V to -40 V in 0.5 V increments. Transfer characteristics of the electrolyte gated devices were acquired at V_{DS} = -1 V while V_{GS} was stepped from 0 V to -3 V in 1mV increments. This gate bias range is chosen to avoid any electrochemical reaction within the electrolyte, while the slow sweep rate is required to let ion move within the viscous gel matrix. The saturation-regime values had been extracted from the slope of $I_{DS}^{1/2}$ (V_{GS}) curves according to equation (1) [5]:

$$I_{DS} = (W/2L)\ \mu_{sat}\ C_i(V_{GS}-V_{th})^2 \qquad (1)$$

Where I_{DS} is the source-drain current, W is the channel width, L is the channel length, μ_{sat} is saturation mobility, C_i is the capacitance per unit area of the dielectric layer, V_{GS} is the source-gate voltage, and V_{th} is the threshold voltage. On/Off current ratio (I_{on}/I_{off}) was determined from the I_{DS} at V_{GS}=0V (I_{off}) and V_{GS}=-40V (I_{on}) for BG devices and I_{DS} at V_{GS}=0V (I_{off}) and V_{GS}=-3V (I_{on}) for TG devices.

3. Results and discussion

3.1 Thermal behavior of BTBT and single crystal preparation

The thermal behavior of BTBT was studied by DSC and the thermograms obtained are given in Fig. S2. They present on heating and cooling only one transition at 219°C and 193°C, respectively, with similar transition enthalpies. On further heating, no additional peaks were observed, indicating that this reversible transition can be attributed to the melting point of the derivative.

BTBT Single crystals were prepared from the freshly synthesized compound by a vapor transport deposition (VTD) method, slightly modified in comparison with the classical technique (see experimental part 2.2). This process leads to the rapid growth of large and thin single crystalline platelets perpendicular to the substrate, as shown by POM in Fig. 1 (B). With a size ranging from dozens to hundreds of micrometers, these platelet-like crystals are very flexible and can be easily bended (see insert of Fig. 1 (B)), indicating a sub-micron thickness typically as thin as 150-300 nm [25].

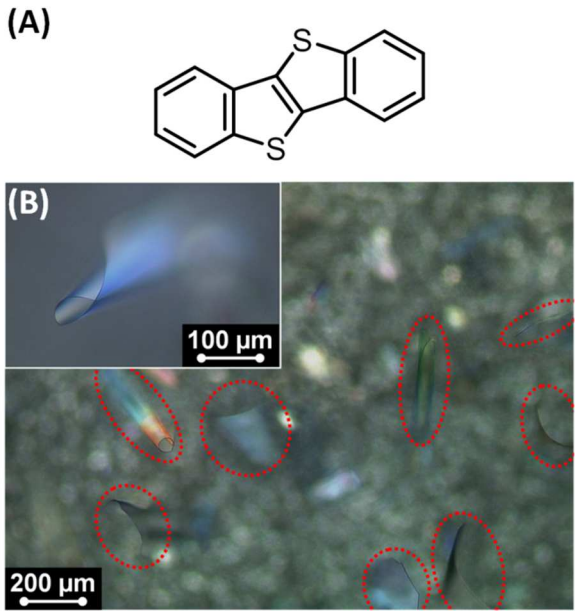

Figure 1. (A) Chemical structure of unsubstituted BTBT core. (B) POM image of BTBT single crystals grown perpendicularly to the top glass substrate (red dashed circles) by vapor transport deposition method. (Insert: magnification of a flexible BTBT single crystal rolled up on itself)

3.2 Single crystal structure analysis

The single crystals of BTBT obtained by vapor transport deposition method were studied by single-crystal XRD. The molecular structure of the unit cell is presented in Fig. 2(A) and the crystallographic data are provided in the Supporting Information (table S1 and cif file). BTBT cores exhibit a layered-herringbone packing as shown in Fig. 2(B). This packing is similar to the one reported previously for BTBT single crystals obtained from solutions by slow liquid/liquid diffusion [26]. This indicates that the molecular packing of BTBT in the crystalline state is not, in that case, sensitive to the crystal growth conditions. This result is also consistent with the simple polymorphism observed by DSC and the absence of crystal-crystal transitions between room temperature and the melting point. This suggests strong van der Waals bonding between crystallized BTBT molecules and the existence of a single crystalline structure.

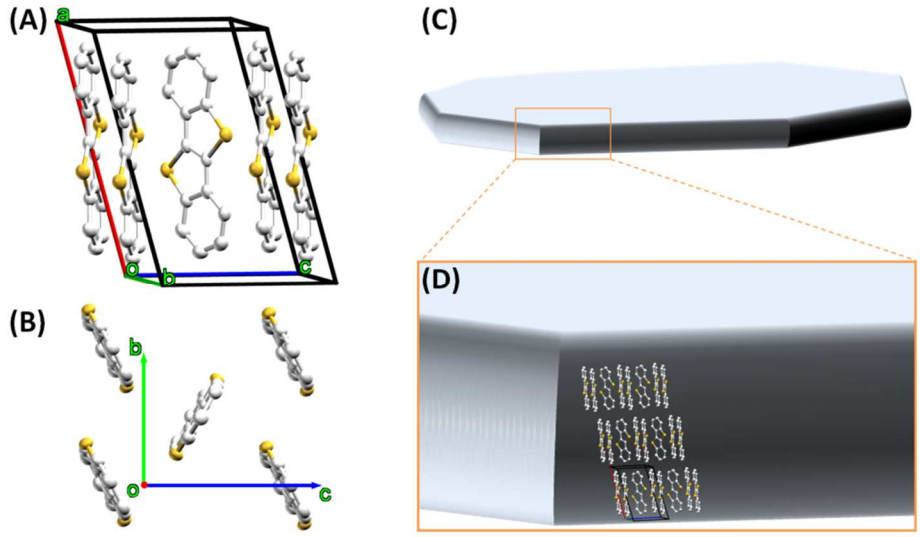

Figure 2. (A) Perspective view of the BTBT crystal structure prepared by vapor transport deposition method. (B) Representation of the herringbone packing structure of BTBT along *a* axis. (C) Schematic representation of the typical platelet-like single-crystals of BTBT obtained by vapor transport deposition method and (D) schematic representation of the lattice and molecular orientation of BTBT cores within the platelet-like crystal. b and c axis are in the plane of the crystal.

To go further into the description of the molecular packing of BTBT single crystals, XRD analysis of oriented crystals was performed (Fig. S3). Large and thin crystals were illuminated with the incident X-ray beam either perpendicular or parallel to the larger facets of the crystals. This procedure gives precious information on the orientation of the unit cell within the crystal and the crystallographic axes can be correlated with the anisotropic shape of the crystals (Fig. S3 (C)). As a result, the longest axis (*a* =11.80 Å) of the unit cell was found to be perpendicular to the larger facets of the crystal, corresponding to the smallest dimension of the platelet, while b and c axis are in the plane. It can be inferred that the BTBT molecules are oriented perpendicular to the larger facets of the crystal and that the layers formed by the herringbone packing of BTBT are in the plane, as illustrated in the Fig. 2(D). This molecular organization is typical for organic crystals obtained by vapor transport deposition. During the growth process, the larger crystal dimension corresponds to the direction of the strongest molecular interactions which corresponds, in the present case, to the strong overlap between the π-conjugated systems of adjacent BTBT molecules. It is important to notice that this molecular packing with the layered-herringbone packing of BTBT in the plane of the crystals is perfectly suitable for the fabrication of single crystal FETs because in such devices the molecular layers will coincide with the direction of the highest mobility of field-induced carriers. However, it is also important to mention that the crystallographic axis in the plane of the herringbone structure (*b* and *c* here) are larger than the ones of alkyl-substituted BTBTs [27]. This indicates that the lack of alkyl chains significantly reduces the intermolecular interactions between the BTBT cores and consequently their potential charge transport properties. This observation is consistent with the modest calculated mobility values of the unsubstituted BTBT derivative (ranging from 10^{-3} to 10^{-1} $cm^2V^{-1}s^{-1}$), in comparison with the ones of alkyl-substituted BTBTs.[15]

3.3 Single crystal morphology and SCOFET fabrication

The quality of BTBT single crystals prepared by vapor transport deposition method was investigated by POM. Based on this optical inspection, the largest birefringent crystals with uniform colors under the crossed polarized light were selected, transferred and deposited with micro-scale gold wire on interdigitated gold electrodes of prefabricated BC/BG FETs, as displayed in Fig. 3(A) and 3(B) (see also Fig. S4). The high flexibility of the BTBT single crystals induced a high quality of the electrostatic bonding to the electrodes and channels of the transistor as confirmed by the POM image in Fig. 3(B). The device structure and the adhesion of the crystal were also checked by SEM and no bends or folds were observed (Fig. 3(C)).

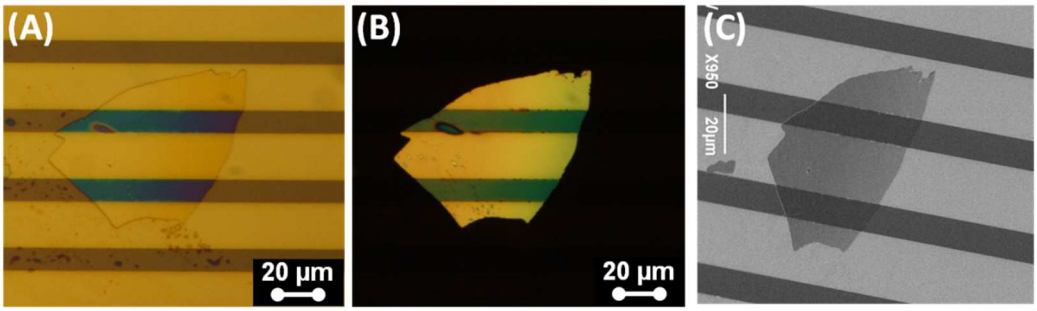

Figure 3. POM images of the single crystal on prefabricated BC/BG transistor (A) under the natural light and (B) under crossed polarized light. (C) SEM image of the device structure.

The morphology of the single crystal onto the transistor was investigated by AFM. The 3D image given in Fig. 4(A) shows the different components of the device such as the crystal, the channel and the gold electrode. The 2D topography image of the crystal (Fig. 4(B)) shows that its surface is rather smooth and that its thickness is about 300 nm according to the height profile of the crystal edge given in the inset of Fig. 4(B). This thickness is consistent with the high flexibility of the single crystal observed by POM during their manipulation and transfer on the transistor structure. At higher magnification (Fig. 4(C)), the top of the crystal presents a layered structure with the presence of terraces. The height of these terraces is about 1.1 nm, or multiples of 1.1 nm, and corresponds to the length of standing molecules. Note that this observation is consistent with the molecular orientation determined by XRD with the layered-herringbone packing of BTBT in the plane of the crystals.

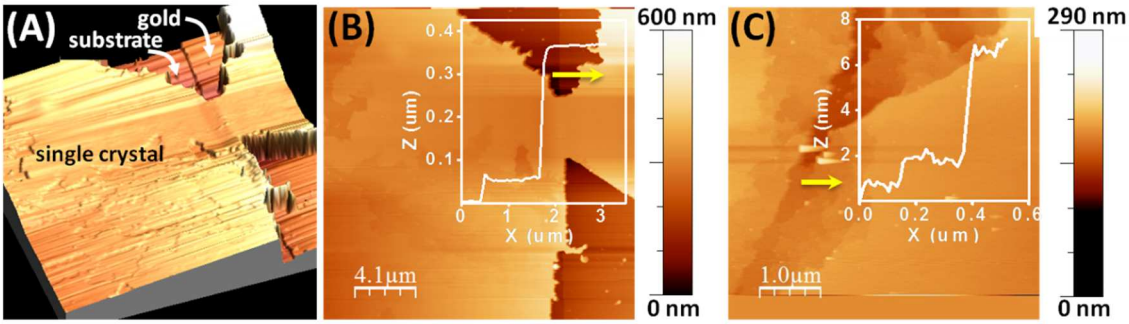

Figure 4. AFM images of BTBT single-crystal deposited on prefabricated BC/BG transistor: (A) 3D topography image. (B) 2D topography image (Inset: height profile of the crystal edge along the yellow arrow. (C) 2D topography image at higher magnification of the top of the single crystal (Inset: terrace step profile along the yellow arrow).

3.4 Charge transport properties of BTBT single crystals

To evaluate the charge carrier mobility of the BTBT single crystal, BC/BG OFET devices with gold electrodes and SiO_2 gate dielectric were first fabricated and characterized. Considering the energy of the highest occupied molecular orbital (HOMO) of BTBT derivatives [28], gold contacts are well-suited for hole injection and charge transport investigation. Fig. 5(A) and (B) show typical transfer and output characteristics of such transistors. From these curves, it can be seen that the devices show a rise of conductance under hole injection (*i.e.* negative gate bias) consistent with a p-channel conduction. An average hole mobility about $2.9x10^{-3}$ $cm^2V^{-1}s^{-1}$ was extracted from saturation regime of a ten of transistors (Fig. S5(A)). The other device parameters such as the average threshold voltage (V_{th}) or average on/off current ratio (I_{on}/I_{off}) are given in Table 1.

To enhance the devices performances, single-crystal OFETs were also prepared with n-octadecyltrichlorosilane (OTS) treated surfaces. The use of an OTS self-assembled monolayer (SAM) on the surface of SiO_2 gate dielectric offers a lower surface energy [29], reduces the water adsorption [30] and decreases the charge trap density at the interface between the crystal and the dielectric [31]. Fig. 5(C) and (D) show typical transfer and output characteristics of an OTS-modified BC/BG OFET. As a result, this surface treatment increased both the mobility and I_{on}/I_{off} by one order of magnitude leading to average values about $1.2x10^{-2}$ $cm^2V^{-1}s^{-1}$ and $2.7x10^4$, respectively. All the device parameters of OTS-modified SCOFETs are summarized in Table 1. Note that all the mobilities were also extracted from saturation regimes of a set of ten transistors (Fig. S5(B)) and that a maximum value as high as $3.2x10^{-2}$ $cm^2V^{-1}s^{-1}$ was measured. Such FET values between 10^{-2} and 10^{-1} $cm^2V^{-1}s^{-1}$ are in good agreement with BTBT calculated mobilities predicted from X-ray crystal structure and ranging from 10^{-3} to 10^{-1} $cm^2V^{-1}s^{-1}$ [15]. They also confirm the good interfacial contact of single-crystals to the dielectric interface as suggested, for instance, by the POM observation during the crystal deposition (see part 3.3).

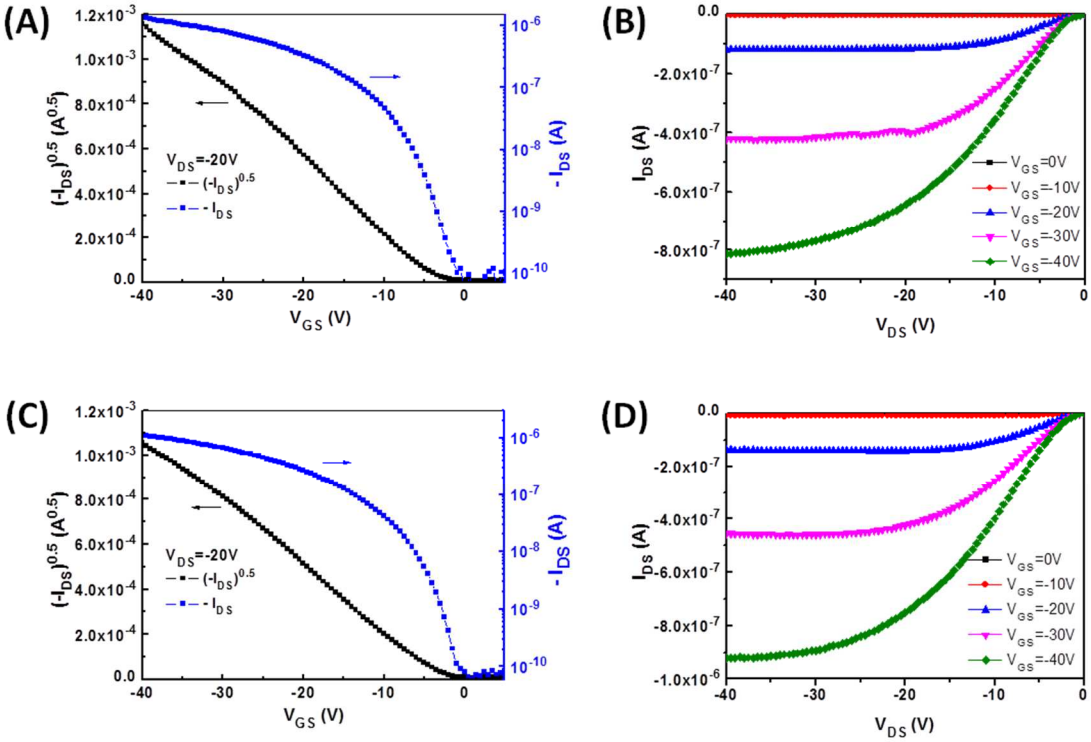

Figure 5. Transfer (A) and output (B) characteristics of BC/BG BTBT single crystal OFET with SiO_2 surface; Transfer (C) and output (D) characteristics of BC/BG BTBT single crystal OFET with OTS treated surface. (The channel width was determined from POM images, and we took care that the values chosen minimize the calculated mobility values.)

Table 1. Summary of the electrical characteristics of BC/BG BTBT SCOFETs.

Surface	μ_h ($cm^2V^{-1}s^{-1}$)[a,b]	V_{th} (V)[b]	I_{ON}/I_{OFF} (VDS=-20V)[b]
SiO_2	(2.9±1.5)X10^{-3}	-(3.1±2.5)	(4.1±2.5) X10^3
OTS	(1.2±0.8) X10^{-2}	-(5.7±1.8)	(2.7±2.6) X10^4

[a] from saturation regime. [b] Average values based on a ten of SCOFET devices.

The air stability of the devices was also investigated. To this end, SCOFETs were removed from the glove box and electrical measurements were performed in ambient conditions. The devices measured in air present a significant degradation of their performances as illustrated in Fig. S6(B). The source-drain current flowing in the crystal is drastically reduced and the mobility is typically decreased by two or three orders of magnitude. The collapse of the mobility can be explained by the diffusion of water present in ambient air in the crystal lattice that is known to form trapping sites for injected charges [32]. This assumption is also supported by the observation of the reversibility of the process since similar device performances can be restored by measuring again the transistors in glove box atmosphere after ambient air condition exposure (Fig. S6(C)).

In addition, SCOFETs with ion gels top gate (TG) configuration were also investigated to reduce voltage operation. Indeed using electrolyte gating, the gate capacitance per unit area is no longer given by the ratio of the dielectric constant over the dielectric thickness but by the ratio of the dielectric constant divided by the ionic double layer thickness. Made of ions, the

latter is typically 1 nm thick, leading to exceptionally high gate capacitance (μF/cm^2) [31-[34]33]. For that purpose, the BTBT single-crystals of BC/BG transistors previously fabricated with SiO_2 or OTS-modified gate dielectric were covered by an ion gel electrolyte consisting in a mixture of a polyethylene glycol (PEG) polymer and a $LiClO_4$ lithium salt (Fig. S1(C)) [24]. Finally, a metallic grid was deposited on the electrolyte drops as gate electrodes. Fig. 6 (and Fig. S7) shows typical transfer and output characteristics of such transistors. In spite of the larger gate capacitance, only a p-type conduction signal was measured. As observed in the output characteristics at five different gate voltage (V_{GS}), the devices show the gate modulation of the source-drain current (I_{DS}) in both the linear and saturation regimes. Thanks to the increase of the gate capacitance, the modulation of the drain source current over three order of magnitude was achieved under 3 V of gate bias (Fig. S7(A) and Fig. 6(A)), while 30 V was required using the conventional SiO_2 dielectric gating. Note that we have been unable to accurately determine a filed effect mobility in this configuration since this will have required an accurate determination of the capacitance value and thus the introduction of a fourth electrode to uncouple the current and potential control.

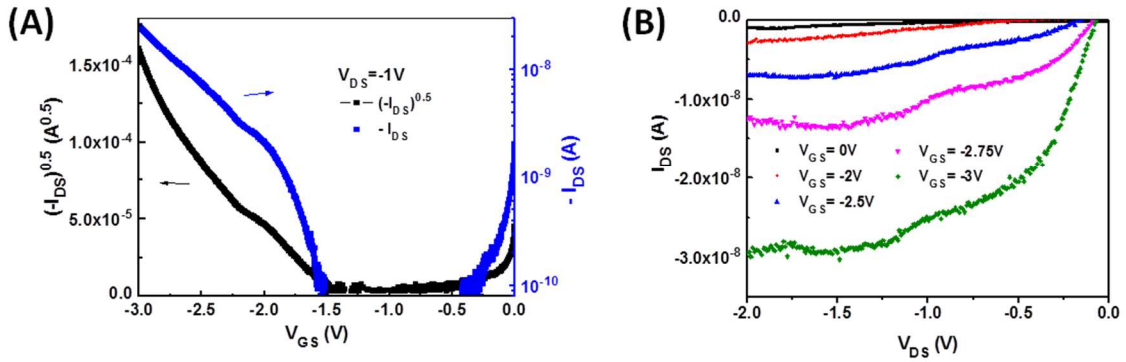

Figure 6. Transfer (A) and output (B) characteristics of BTBT TG single crystal OFET with OTS treated surface.

4. Conclusions

In summary, we prepared thin single crystals of an unsubstituted BTBT by physical vapor transport deposition technique. The structure and morphology analysis of these platelet-like crystals demonstrated that the BTBT aromatic cores are oriented perpendicular to the larger facets of the crystal and that they are organized in a layered herringbone packing in the plane. The charge transport properties of BTBT single-crystals were investigated by BC/BG organic field-effect transistors on both SiO_2 and OTS-treated gate dielectric, and a maximum hole mobility value of 0.032 cm^2 V^{-1} s^{-1} was measured, in good agreement with calculated mobilities predicted from the BTBT crystal structure and reported in the literature. In addition, ion gels TG OFETs based on BTBT single crystals were also fabricated to generate low operating gate voltages. This work presents the first investigation of charge carrier mobility of simple BTBT aromatic core in transistor configuration and corroborates the crucial role of the BTBT substitution to achieve high charge transport properties with such derivatives.

Acknowledgments

This work was supported by the China Scholarship Council, China, and the CNRS (PICS N°88085), France. The work has been made possible thanks to emergence funding from Sorbonne University and is also supported by the European Research Council (ERC) starting grant (blackQD, 756225).

Appendix A. Supplementary material

Supplementary data associated with this article can be found, in the online version, at http://dx.doi.org/

References

[1] S.R. Forrest, The path to ubiquitous and low-cost organic electronic appliances on plastic, Nature. 428 (2004) 911–918. https://doi.org/10.1038/nature02498.

[2] J.H. Burroughes, D.D.C. Bradley, A.R. Brown, R.N. Marks, K. Mackay, R.H. Friend, P.L. Burns, A.B. Holmes, Light-emitting diodes based on conjugated polymers, Nature. 347 (1990) 539–541. https://doi.org/10.1038/347539a0.

[3] Y. Yao, L. Zhang, T. Leydecker, P. Samorì, Direct Photolithography on Molecular Crystals for High Performance Organic Optoelectronic Devices, J. Am. Chem. Soc. 140 (2018) 6984–6990. https://doi.org/10.1021/jacs.8b03526.

[4] L.A. Morrison, D. Stanfield, M. Jenkins, A.A. Baronov, D.L. Patrick, J.M. Leger, High performance organic field-effect transistors using ambient deposition of tetracene single crystals, Org. Electron. Physics, Mater. Appl. 33 (2016) 269–273. https://doi.org/10.1016/j.orgel.2016.03.021.

[5] J. Zaumseil, H. Sirringhaus, Electron and ambipolar transport in organic field-effect transistors, Chem. Rev. 107 (2007) 1296–1323. https://doi.org/10.1021/cr0501543.

[6] Y. Luo, F. Gustavo, J.Y. Henry, F. Mathevet, F. Lefloch, M. Sanquer, P. Rannou, B. Grévin, Probing local electronic transport at the organic single-crystal/dielectric interface, Adv. Mater. 19 (2007) 2267–2273. https://doi.org/10.1002/adma.200700913.

[7] K. Takimiya, I. Osaka, T. Mori, M. Nakano, Organic semiconductors based on [1]benzothieno[3,2-B][1]benzothiophene substructure, Acc. Chem. Res. 47 (2014) 1493–1502. https://doi.org/10.1021/ar400282g.

[8] K. Takimiya, H. Ebata, K. Sakamoto, T. Izawa, T. Otsubo, Y. Kunugi, 2,7-Diphenyl[1]benzothieno[3,2-b]benzothiophene, A New Organic Semiconductor for Air-Stable Organic Field-Effect Transistors with Mobilities up to 2.0 cm 2 V -1 s -1, J. Am. Chem. Soc. 128 (2006) 12604–12605. https://doi.org/10.1021/ja064052l.

[9] H. Ebata, T. Izawa, E. Miyazaki, K. Takimiya, M. Ikeda, H. Kuwabara, T. Yui, Highly Soluble [1] Benzothieno [3 , 2-b] benzothiophene (BTBT) Derivatives for High-Performance, Solution-Processed Organic Field-Effect Transistors, J. Am. Chem. Soc. 129 (2007) 15732–15733. https://doi.org/10.1002/adma.200802031.

[10] H. Minemawari, T. Yamada, H. Matsui, J.Y. Tsutsumi, S. Haas, R. Chiba, R. Kumai, T. Hasegawa, Inkjet printing of single-crystal films, Nature. 475 (2011) 364–367. https://doi.org/10.1038/nature10313.

[11] H. Iino, T. Usui, J.I. Hanna, Liquid crystals for organic thin-film transistors, Nat. Commun. 6 (2015). https://doi.org/10.1038/ncomms7828.

[12] A.Y. Amin, A. Khassanov, K. Reuter, T. Meyer-Friedrichsen, M. Halik, Low-voltage organic field effect transistors with a 2-tridecyl[1] benzothieno[3,2-b][1]benzothiophene semiconductor layer, J. Am. Chem. Soc. 134 (2012) 16548–16550. https://doi.org/10.1021/ja307802q.

[13] Y. Tsutsui, G. Schweicher, B. Chattopadhyay, T. Sakurai, J.B. Arlin, C. Ruzié, A. Aliev, A. Ciesielski, S. Colella, A.R. Kennedy, V. Lemaur, Y. Olivier, R. Hadji, L. Sanguinet, F. Castet, S. Osella, D. Dudenko, D. Beljonne, J. Cornil, P. Samorì, S. Seki, Y.H. Geerts, Charge Carrier Mobility: Unraveling Unprecedented Charge Carrier Mobility through Structure Property Relationship of Four Isomers of Didodecyl[1]benzothieno[3,2-b][1]benzothiophene, Adv. Mater. 28 (2016) 7106-7114. https://doi.org/10.1002/adma.201670233.

[14] H. Minemawari, M. Tanaka, S. Tsuzuki, S. Inoue, T. Yamada, R. Kumai, Y. Shimoi, T. Hasegawa, Enhanced Layered-Herringbone Packing due to Long Alkyl Chain Substitution in Solution-Processable Organic Semiconductors, Chem. Mater. 29 (2017) 1245–1254. https://doi.org/10.1021/acs.chemmater.6b04628.

[15] M. Alkan, I. Yavuz, Intrinsic charge-mobility in benzothieno[3,2- b] [1]benzothiophene (BTBT) organic semiconductors is enhanced with long alkyl side-chains, Phys. Chem. Chem. Phys. 20 (2018) 15970–15979. https://doi.org/10.1039/c8cp01640b.

[16] H. Ebata, E. Miyazaki, T. Yamamoto, K. Takimiya, Synthesis, properties, and structures of benzo[1,2-b:4,5-b']bis[b] benzothiophene and benzo[1,2-b:4,5-b']bis[b]benzoselenophene, Org. Lett. 9 (2007) 4499–4502. https://doi.org/10.1021/ol701815j.

[17] R.A. Laudise, C. Kloc, P.G. Simpkins, T. Siegrist, Physical vapor growth of organic semiconductors, J. Cryst. Growth. 187 (1998) 449–454. https://doi.org/10.1016/S0022-0248(98)00034-7.

[18] M. Saito, I. Osaka, E. Miyazaki, K. Takimiya, H. Kuwabara, M. Ikeda, One-step synthesis of [1]benzothieno[3,2-b][1]benzothiophene from o-chlorobenzaldehyde, Tetrahedron Lett. 52 (2011) 285–288. https://doi.org/10.1016/j.tetlet.2010.11.021.

[19] O. V. Dolomanov, L.J. Bourhis, R.J. Gildea, J.A.K. Howard, H.J. Puschmann, OLEX2: a complete structure solution, refinement and general all round good thing Olex2, J. Appl. Crystallogr. 42 (2009) 339–341. https://doi.org/doi:10.1107/S0021889808042726.

[20] G.M. Sheldrick, SHELXT--Integrated space-group and crystal-structure determination, Acta Crystallogr. Sect. A:Foundations and advances. 71 (2015) 3–8. https://doi.org/10.1107/S2053273314026370.

[21] G.M. Sheldrick, Crystal structure refinement with SHELXL, Acta Crystallogr. Sect. C: Structural chemistry. 71 (2015) 3–8. https://doi.org/10.1107/S2053229614024218.

[22] M. Lessel, O. Bäumchen, M. Klos, H. Hähl, R. Fetzer, M. Paulus, R. Seemann, K. Jacobs, Self-assembled silane monolayers: An efficient step-by-step recipe for high-quality, low energy surfaces, Surf. Interface Anal. 47 (2015) 557–564. https://doi.org/10.1002/sia.5729.

[23] E. Lhuillier, S. Ithurria, A. Descamps-Mandine, T. Douillard, R. Castaing, X.Z. Xu, P.L. Taberna, P. Simon, H. Aubin, B. Dubertret, Investigating the n- and p-Type Electrolytic Charging of Colloidal Nanoplatelets, J. Phys. Chem. C. 119 (2015) 21795–21799. https://doi.org/10.1021/acs.jpcc.5b05296.

[24] E. Lhuillier, S. Pedetti, S. Ithurria, H. Heuclin, B. Nadal, A. Robin, G. Patriarche, N. Lequeux, B. Dubertret, Electrolyte-gated field effect transistor to probe the surface defects and morphology in films of thick CdSe colloidal nanoplatelets, ACS Nano. 8 (2014) 3813–3820. https://doi.org/10.1021/nn500538n.

[25] A.L. Briseno, R.J. Tseng, M.-M. Ling, E.H.L. Falcao, Y. Yang, F. Wudl, Z. Bao, High-Performance Organic Single-Crystal Transistors on Flexible Substrates, Adv. Mater. 18 (2006) 2320–2324. https://doi.org/10.1002/adma.200600634.

[26] V.S. Vyas, R. Gutzler, J. Nuss, K. Kern, B. V. Lotsch, Optical gap in herringbone and π-stacked crystals of [1]benzothieno[3,2-b]benzothiophene and its brominated derivative, CrystEngComm. 16 (2014) 7389–7392. https://doi.org/10.1039/c4ce00752b.

[27] T. Izawa, E. Miyazaki, K. Takimiya, Molecular ordering of high-performance soluble molecular semiconductors and re-evaluation of their field-effect transistor characteristics, Adv. Mater. 20 (2008) 3388–3392. https://doi.org/10.1002/adma.200800799.

[28] H. Kobayashi, N. Kobayashi, S. Hosoi, N. Koshitani, D. Murakami, R. Shirasawa, Y. Kudo, D. Hobara, Y. Tokita, M. Itabashi, Hopping and band mobilities of pentacene, rubrene, and 2,7-dioctyl[1] benzothieno[3,2-b][1]benzothiophene (C8-BTBT) from first principle calculations, J. Chem. Phys. 139 (2013) 014707. https://doi.org/10.1063/1.4812389.

[29] K. Shankar, T.N. Jackson, Morphology and electrical transport in pentacene films on silylated oxide surfaces, J. Mater. Res. 19 (2004) 2003–2007. https://doi.org/10.1557/JMR.2004.0255.

[30] H.S. Seo, Y.S. Jang, Y. Zhang, P. Syed Abthagir, J.H. Choi, Fabrication and characterization of pentacene-based transistors with a room-temperature mobility of 1.25 cm2/Vs, Org. Electron. Physics, Mater. Appl. 9 (2008) 432–438. https://doi.org/10.1016/j.orgel.2008.01.008.

[31] C. Goldmann, D.J. Gundlach, B. Batlogg, Evidence of water-related discrete trap state formation in pentacene single-crystal field-effect transistors, Appl. Phys. Lett. 88 (2006) 63501. https://doi.org/10.1063/1.2171479.

[32] O.D. Jurchescu, J. Baas, T.T.M. Palstra, Electronic transport properties of pentacene single crystals upon exposure to air, Appl. Phys. Lett. 87 (2005) 052102. https://doi.org/10.1063/1.2001130.

[33] H. Shimotani, H. Asanuma, J. Takeya, Y. Iwasa, Electrolyte-gated charge accumulation in organic single crystals, Appl. Phys. Lett. 89 (2006) 203501. https://doi.org/10.1063/1.2387884.

[34] M.J. Panzer, C.D. Frisbie, Polymer electrolyte-gated organic field-effect transistors: Low-voltage, high-current switches for organic electronics and testbeds for probing electrical transport at high charge carrier density, J. Am. Chem. Soc. 129 (2007) 6599–6607. https://doi.org/10.1021/ja0708767.

[35] J.H. Cho, J. Lee, Y. Xia, B. Kim, Y. He, M.J. Renn, T.P. Lodge, C. Daniel Frisbie, Printable ion-gel gate dielectrics for low-voltage polymer thin-film transistors on plastic, Nat. Mater. 7 (2008) 900–906. https://doi.org/10.1038/nmat2291.